Interlayer Polarization Beam Splitter Based on Asymmetrical Si Wire Directional Coupler

Yuki Atsumi, *Member, IEEE*, Ryohei Takei, *Member, IEEE*, Makoto Okano, *Member, IEEE*, Tomohiro Amemiya, *Member, IEEE*, Youichi Sakakibara, and Masahiko Mori

Abstract—We proposed and designed a compact Si interlayer polarization beam splitter (PBS) that is based on a crystalline Si and hydrogenated amorphous Si (a-Si:H) vertical asymmetrical directional coupler toward 3-D Si photonics integrated circuits. The changeable thickness of the upper a-Si:H waveguide enables the realization of the TM-mode-coupled PBS with simple-structured parallel Si wire waveguides. The device with a 260-nm × 220-nm first-layer waveguide and a 340-nm × 200-nm second-layer waveguide operates in a broadband width of 77 nm, with a crosstalk of less than −20 dB and an insertion loss of <0.3 dB in the *C*-band. The device is robust in terms of alignment error between the two waveguides.

Index Terms—Photonic integrated circuits, polarization beam splitter, silicon photonics, vertical directional coupler.

I. INTRODUCTION

SILICON photonics integrated circuits (Si-PICs) have the potential to provide high-density signal transmission for intra-chip interconnection in a datacenter or a large-scale routing system that is part of a next-generation optical path network, and do so with low electricity consumption [1], [2]. Recently, multilayered three-dimensional (3D) Si-PICs have been researched for the sake of enhancing flexibility of circuit architecture and for partial waveguide bridges to reduce the insertion loss of the numerous waveguide crossings in the circuits [3]. For the 3D Si-PICs, the use of hydrogenated amorphous silicon (a-Si:H) as an upper layer is promising because of their compatibility with the low-temperature CMOS back-end process. To date, a high-quality a-Si:H film with low infrared optical absorption was realized, and waveguides with propagation losses of as small as 0.6 dB/cm for a ridge type [4] and 1.1 dB/cm for a wire type [5] which was comparable with that of c-Si waveguide have been demonstrated. Also, some interlayer optical transmitters with intensive polarization or high coupling efficiency have been demonstrated [6]–[8].

Thus, fundamental technologies of 3D Si-PICs have been promisingly improved. Then, a next important research target of 3D Si-PICs would be to manage polarization of the light. An interlayer polarization beam splitter (PBS) would be one

of the interesting polarization management tools because it separates the mixed-polarization signals into each polarization for the different layers in the 3D Si-PICs. Then, the PBSs can be used to configure the polarization diversity and polarization division multiplexing (PDM) systems which execute signal processing in different layers for each polarization. However, the a-Si:H based interlayer PBSs have not been reported yet.

In this letter, we designed an interlayer PBS based on a vertical asymmetrical directional coupler (ADC). The ADC-PBS consists of two waveguides with different dimensions selected to satisfy correspondence between the effective indices for TM polarization and well-separation between those for the TE polarization. Therefore, the TM-mode light performs directional coupling while the TE-mode light goes through the input port [9], [10]. The vertical ADC structure is formed by the alternate stacking process of a-Si:H and SiO_2 cladding layers using the plasma-enhanced chemical vapor deposition (PECVD). Then, the thickness of the upper a-Si:H waveguide can be changed along with the widths of both layered waveguides. This enhances the flexibility in parameters to control the effective indices of the TE and TM modes for the 2nd-layer waveguide. Thus, the simple-structured vertical PBSs with straight parallel Si wire waveguides can be realized. Meanwhile, the vertical ADC-PBS is subject to degradation by the error in dimensions, especially in the thickness of the upper a-Si:H layer and alignment between the two waveguides. Therefore, we also evaluated the sensitivity of the vertical interlayer ADC-PBS to error in the device dimensions.

II. DEVICE STRUCTURE AND DESIGN

Fig. 1(a) is the schematic of the proposed interlayer PBS comprising the ADC, the bending waveguides, and the thickness and width converters. The 1st- and 2nd-layer waveguides are fabricated with c-Si and a-Si:H, respectively, on a SOI substrate. The input and output ports are 220 nm thick, so they can connect with commonly used PICs. Fig. 1(b) shows the cross-sectional dimensions of the ADC that are set according to the parameters W_1, W_2, and H_2, which are controlled through the fabrication process. The parameters are determined so as to satisfy the previously described PBS criterion, i.e., the difference between the N_{eff-TE} of the 1st- and 2nd-layer waveguides is large and the N_{eff-TM} of them are coincident.

The TE- and TM-mode light enters the 2nd-layer waveguide, the width of which is W_2 and its thickness is reduced from 220 nm to H_2 using a diagonally etched thickness converter of length L_T as shown in Fig. 1(c). In the ADC section,
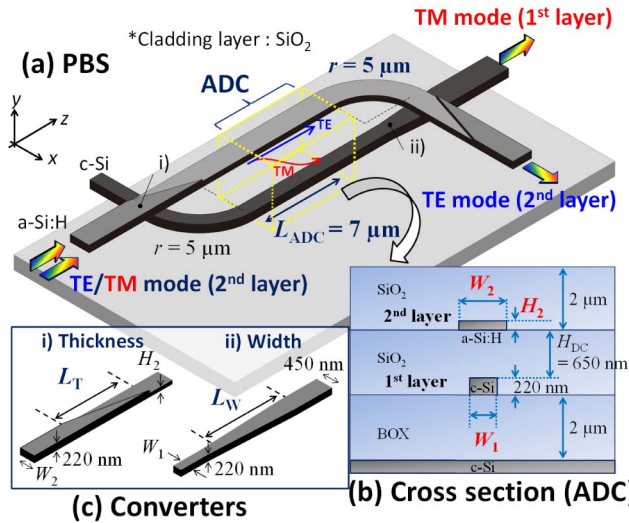
Fig. 1. (a) Overall structure of the proposed PBS. The TE- and TM-polarized lights are input from the 2nd-layer waveguide. (b) Cross section of the ADC section of the PBS. The parameters W_1, W_2, and H_2 are determined to satisfy the criterion for the PBS. (c) Schematics of the thickness and width converters.
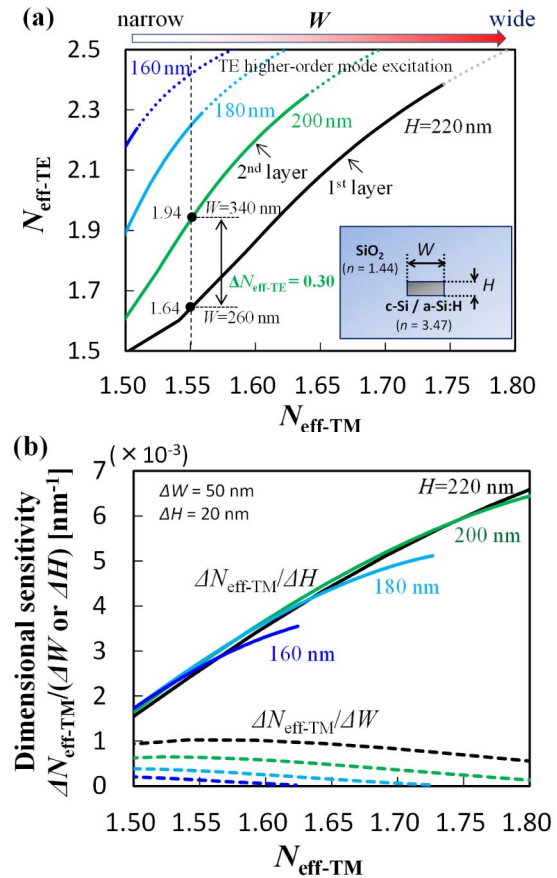

Fig. 2. (a) Relationship between N_{eff} for the fundamental modes of TE and TM of the Si wire waveguides for different thicknesses. The refractive indices of c-Si, a-Si:H and SiO_2 are $n_{c-Si} = n_{a-Si:H} = 3.47$, and $n_{SiO2} = 1.44$ at a wavelength of 1.55 μm. (b) Dimensional sensitivity for N_{eff-TM} of the Si wire waveguides. As for TM mode, thickness error strongly affects the effective index compared to width error.

the TE-mode light goes through the 2nd-layer waveguide and the TM-mode light couples to the 1st-layer waveguide of width W_1. Next, the light in the 2nd-layer waveguide is guided out by a bending waveguide that reconnects to the 220-nm-thick waveguide via the converter. Meanwhile, W_1 of the 1st-layer waveguide is converted to 450 nm by a width converter of length L_W after the waveguide emerges from the ADC.

Fig. 2(a) shows the relationship between the effective indices for the TE and TM fundamental modes of the Si wire waveguides for various waveguide thicknesses. The thickness of the 1st-layer c-Si waveguide was set at $H = 220$ nm. Arbitrary pairs of waveguides that have different thicknesses but the same N_{eff-TM} can be used in the PBS. Then, the difference between the N_{eff-TE} of the two waveguides, ΔN_{eff-TE}, suppresses the TE-mode polarization crosstalk. The ΔN_{eff-TE} can be increased by introducing a thinner 2nd-layer waveguide. However, a thinner 2nd-layer waveguide requires a longer L_T in the thickness converter, so the 2nd-layer waveguide was designed such that $H_2 = 200$ nm. In addition, the interlayer distance, H_{DC}, also affects polarization crosstalk. In general, as the interlayer distance increases, the crosstalk decreases. On the other hand, a large H_{DC} increases the TM-mode coupling length. The H_{DC} was set to 650 nm to decrease the crosstalk to less than −20 dB at the general spatial waveguide crossings [11].

Each combination of N_{eff-TM} and N_{eff-TE} determines a unique set of cross-sectional waveguide dimensions, and as N_{eff-TM} increases, the width increases. The wide waveguides are subject to excitation in the higher-order mode of TE polarization, as indicated by the dotted lines on the curves in Fig. 2(a). On the other hand, a small N_{eff-TM} is close to the mode-cutoff boundary. We used $N_{eff-TM} = 1.55$ because a waveguide with a small N_{eff-TM} can achieve broadband PBS operation and is relatively robust for the thickness error, as shown in Fig. 2(b). Therefore, the widths

of the 220-nm-thick 1st-layer waveguide and the 200-nm-thick 2nd-layer waveguide are $W_1 = 260$ nm and $W_2 = 340$ nm with N_{eff-TE} of 1.64 and 1.94, respectively. Moreover, the length of the ADC, L_{ADC}, was calculated to be 7 μm to adjust the center wavelength of the directional coupler for the TM-mode to 1.55 μm.

Next, we evaluated the radiation loss caused by a 90° bend in the 2nd-layer waveguide with a core size of 340 nm × 200 nm using the 3D-finite-difference time-domain (3D-FDTD) method. As shown in Fig. 3, the allowable bending radius for the TE mode for a loss of <0.1 dB was calculated to be as small as 5 μm. On the other hand, the TM mode had a large radiation loss of 3.6 dB at that bending radius because optical confinement in the Si core for the TM-mode was weak due to the small N_{eff-TM} of the 2nd-layer waveguide.

The thickness converter for the 2nd layer and the width converter for the 1st layer were designed using the eigen-mode expansion (EME) method with the wavelength of 1550 nm. For the former, when $L_T \geqslant 10$ μm, the polarization rotation is suppressed to be less than −20 dB and the insertion loss is <0.01 dB for the both polarized modes. For the latter, when $L_W \geqslant 10$ μm, the insertion loss is <0.01 dB. By using these values, the ADC can be connected to commonly used
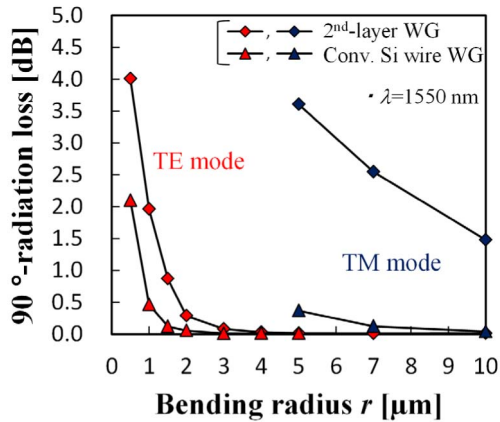
Fig. 3. Bending losses of a 340-nm × 200-nm 2nd-layer waveguide and a conventional 450-nm × 220-nm Si wire waveguide.

220-nm-thick PICs. Totally, the proposed interlayer ADC-PBS can be fabricated to be as small as 20 μm × 30 μm including these converters, and has an advantage in device footprint over the serial arrangement of the conventional in-plane PBS and interlayer beam transmitter which achieves the interlayer PBS operation [9], [10], [12], [13].

III. DEVICE CHARACTERISTICS AND DISCUSSION

Transmission characteristics of the designed ADC-PBS were evaluated by the 3D-FDTD method. The thickness and width converters were not included in the simulation model, i.e., the dimensions of the input and output ports for the 1st- and 2nd-layer waveguides were 260 nm × 220 nm and 340 nm × 200 nm, respectively. The simulation model includes material dispersion, and the calculated TE- and TM-polarized fundamental modes were separately input. The minimum grid sizes for calculation were 10 and 2 nm in the direction of waveguide width (x) and thickness (y), respectively at the waveguide interfaces. The grid sizes were gradually increased to 40 and 20 nm with the rate of 10%. On the other hand, the size for the propagating direction (z) was fixed at 20 nm. Fig. 4 (a) shows the transmission for dominant polarizations. The insertion losses for the TE and TM modes were <0.03 dB and <0.3 dB in the C-band (1530–1565 nm), respectively. The minimum insertion loss for the TM mode mainly arose from a mismatch in $N_{\text{eff}-\text{TM}}$ for the both waveguides. The spectrum of the TE mode curved downward for longer wavelengths because of the optical coupling to cross port and the intrinsic 5-μm-radius bending loss in the 2nd layer as shown by the gray line. Fig. 4(b) describes the transmission for minor polarizations. The dotted lines represent the base lines for crosstalk of −20 dB against each dominant polarization, and the bandwidth for the TM modes was as wide as 77 nm, which covers the C-band. In that wavelength range, the polarization crosstalk for TE mode was much less than −20 dB, which indicates that the difference between the $N_{\text{eff}-\text{TE}}$ of the 1st- and 2nd-layer waveguides is sufficiently large for the ADC. Moreover, the spectrum of the minor TM mode also curved downward for longer wavelengths due to the intrinsic bending loss. The difference in bending loss between both polarizations decreased the crosstalk for the bar port.
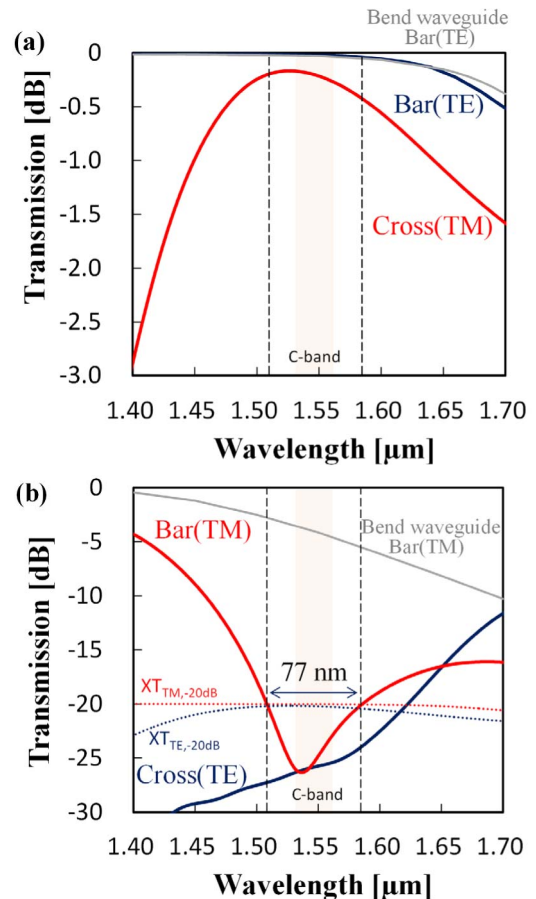

Fig. 4. Transmission of the ADC-PBS as a function of the wavelength; (a) indicates the insertion loss for the dominant polarized light in the both output ports, and (b) discusses the polarization crosstalk (XT). The dotted lines indicate the XT of -20 dB based on each dominant polarization.

High structural sensitivity for Si photonics often makes it difficult to obtain the propagation characteristics for which the structure was designed. Fig. 5(a) shows the insertion loss and the polarization crosstalk in the C-band for the both output ports as a function of the 2nd-layer waveguide thickness error. The TM-mode light was sensitive to error compared to TE mode, and crosstalk of about −20 dB were obtained within plus or minus a few nanometers with insertion loss of <0.5 dB. Actually, It is extremely hard to control a a-Si:H thickness accurately only with PECVD deposition. However, the fine thickness control with a resolution of ⩽1 nm can be achieved by using the endpoint detection for isotropic wet-etching of a-Si:H with an organic alkaline solution after the deposition process [5]. The waveguide thickness for the minimum insertion loss of TM mode mismatched that for the minimum crosstalk because the thin waveguides have a large bending loss for the TM mode compared to that for the thick waveguides, and the losses improve the polarization crosstalk. On the other hand, the mismatch of the $N_{\text{eff}-\text{TM}}$ owing to the dimensional errors of the waveguides degraded the crosstalk and the insertion loss. Thus, the total of these effects might generate a mismatch.

Fig. 5(b) shows the dependence of the insertion loss and the crosstalk on the width errors of the 1st- and the 2nd-layer waveguides. As for the insertion loss of TM mode, the
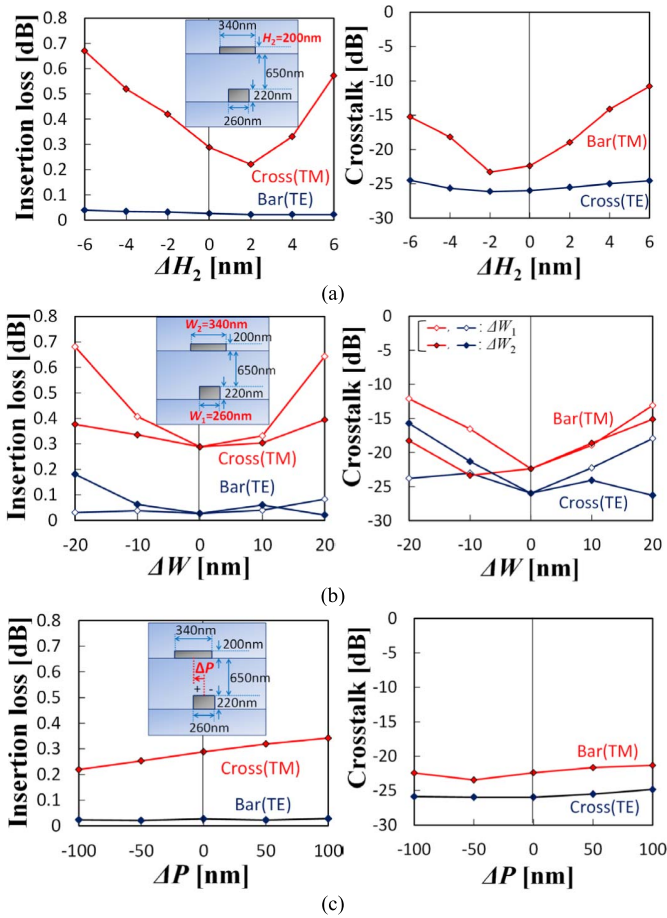
Fig. 5. The insertion loss and the polarization crosstalk for bar and cross ports in the range of the C-band as functions of the error in (a) 2nd-layer waveguide thickness, (b) 1st- and 2nd-layer waveguide widths and (c) 2nd-layer waveguide alignment.

2nd-layer waveguide was more tolerant of the width error than the 1st-layer waveguide because the 2nd-layer waveguide width is larger than that of the 1st layer. The allowable error for the width of the 1st-layer waveguide was about ± 5 nm to achieve a crosstalk of less than -20 dB. In contrast, the 2nd-layer waveguide was more robust for the narrower directional errors because of the larger bending loss for the minor TM mode. For the TE mode, crosstalk became large with increase in W_1 and decreased in W_2 because the $\Delta N_{\mathrm{eff-TE}}$ between the two waveguides becomes small.

Fig. 5(c) shows the dependence of the insertion loss and the crosstalk on misalignment of the 1st- and 2nd-layer waveguides. The misalignment leads to increase of the interlayer distance and weakens the modal coupling coefficient for both waveguides. Therefore, the center wavelength for the ADC is redshifted. In the error range of more than ± 100 nm, the crosstalk was less than -20 dB because the bandwidth of the PBS was sufficient wide compared to the amount of redshift for TM mode in Fig. 4(b). In addition, the insertion loss for TM mode was <0.4 dB.

IV. CONCLUSION

In this letter, we proposed a Si interlayer PBS that is based on a vertical ADC for use with multilayered Si-PICs.

A simple-structured PBS with straight parallel Si wire waveguides was designed by adjusting the thickness of the upper-layer a-Si:H waveguide and the widths of both waveguides. In terms of mitigation of thickness error sensitivity and broadband operation, the 1st- and 2nd-layer waveguides for the ADC were designed to be 260 nm $\times$ 220 nm and 340 nm $\times$ 200 nm, respectively. To have the waveguides connect with commonly used 220-nm-thick PICs, we added a 5-μm-radius bending waveguide for the 2nd layer and 10-μm-long thickness and width converters. For the PBS, we obtained a 77-nm bandwidth with crosstalk of less than -20 dB and insertion loss of <0.3 dB in the C-band. In addition, we evaluated the sensitivity of the PBS to error in waveguide dimensions, and the allowable thickness error for the 2nd-layer waveguide was within plus or minus a few nanometers, which was controllable using endpoint detection of isotropic wet-etching. Moreover, the PBS showed high robustness with respect to the alignment error of the waveguides.

This interlayer ADC-PBS is configured with the size of as small as 20 μm $\times$ 30 μm, and we believe that it will be used in 3D-PICs in the near future.

REFERENCES

[1] R. Soref, "The past, present, and future of silicon photonics," *IEEE J. Sel. Topics Quantum Electron.*, vol. 12, no. 6, pp. 1678–1687, Nov./Dec. 2006.

[2] K. Tanizawa *et al.*, "Ultra-compact 32 × 32 strictly-non-blocking Si-wire optical switch with fan-out LGA interposer," *Opt. Exp.*, vol. 23, no. 13, pp. 17599–17606, Jun. 2015.

[3] A. Biberman *et al.*, "Photonic network-on-chip architectures using multilayer deposited silicon materials for high-performance chip multiprocessors," *ACM J. Emerg. Technol. Comput. Syst.*, vol. 7, Jul. 2011, Art. no. 7.

[4] R. Takei, S. Manako, E. Omoda, Y. Sakakibara, M. Mori, and T. Kame, "Sub-1 dB/cm submicrometer-scale amorphous silicon waveguide for backend on-chip optical interconnect," *Opt. Exp.*, vol. 22, no. 4, pp. 4779–4788, Feb. 2014.

[5] K. Furuya *et al.*, "Nanometer-scale thickness control of amorphous silicon using isotropic wet-etching and low loss wire waveguide fabrication with the etched material," *Appl. Phys. Lett.*, vol. 100, no. 25, p. 251108, Jun. 2012.

[6] R. Sun *et al.*, "Impedance matching vertical optical waveguide couplers for dense high index contrast circuits," *Opt. Exp.*, vol. 16, no. 16, pp. 11682–11690, Jul. 2008.

[7] J. H. Kang *et al.*, "Amorphous-silicon inter-layer grating couplers with metal mirrors toward 3-D interconnection," *IEEE J. Sel. Topics Quantum Electron.*, vol. 20, no. 4, Jul./Aug. 2014, Art. no. 8202308.

[8] R. Takei, Y. Maegami, E. Omoda, Y. Sakakibara, M. Mori, and T. Kame, "Low-loss and low wavelength-dependence vertical interlayer transition for 3D silicon photonics," *Opt. Exp.*, vol. 23, no. 14, pp. 18602–18610, Jul. 2015.

[9] S. Lin, J. Hu, and K. B. Crozier, "Ultracompact, broadband slot waveguide polarization splitter," *Appl. Phys. Lett.*, vol. 98, no. 15, p. 151101, Apr. 2011.

[10] J. Wang, D. Liang, Y. Tang, D. Dai, and J. E. Bowers, "Realization of an ultra-short silicon polarization beam splitter with an asymmetrical bent directional coupler," *Opt. Lett.*, vol. 38, no. 1, pp. 4–6, Jan. 2013.

[11] K. Furuya, R. Takei, T. Kamei, Y. Sakakibara, and M. Mori, "Basic study of coupling on three-dimensional crossing of Si photonic wire waveguide for optical interconnection on inter or inner chip," *Jpn. J. Appl. Phys.*, vol. 51, no. 4S, p. 04DG12, Apr. 2012.

[12] A. Hosseini, S. Rahimi, X. Xu, D. Kwong, J. Covey, and R. T. Chen, "Ultracompact and fabrication-tolerant integrated polarization splitter," *Opt. Lett.*, vol. 36, no. 20, pp. 4047–4049, Oct. 2011.

[13] D. Dai, Z. Wang, J. Peters, and J. E. Bowers, "Compact polarization beam splitter using an asymmetrical Mach–Zehnder interferometer based on silicon-on-insulator waveguides," *IEEE Photon. Technol. Lett.*, vol. 24, no. 8, pp. 673–675, Apr. 15, 2012.